scientific reports

Check for updates

OPEN

Development of co-doped ZnS-CdS quantum dots based composite sensor for the detection of cefixime (CXM) and tetracycline (TET), and application in real samples from local dairies

Shakiba Javaheri[1], Fatemeh Keshavarzi[1]✉ & Changiz Karami[2]

The excessive use of antibiotics, particularly Cefixime (CXM) and tetracycline (TET), poses serious risks to human health and the environment. This study presents a novel detection method utilizing zinc sulfide-cadmium sulfide/cobalt (ZnS-CdS/Co) quantum dots, characterized through scanning electron microscopy (SEM), photoluminescence (PL), energy dispersive X-ray (EDX), mapping, Line scan, Fourier-transform infrared spectroscopy (FT-IR) techniques, and X-ray diffraction (XRD). Aqueous solutions of varied TET and CXM concentrations were prepared and analyzed using these synthesized quantum dots. The analysis revealed a significant decrease in fluorescence intensity with increasing antibiotic concentrations, demonstrating the method's high specificity and sensitivity. Recovery experiments with spiked milk samples yielded high accuracy, with CXM recovery rates ranging from 96.0 to 100.77% for Bistoon milk and 100.5–100.33% for Kalleh milk; TET recovery rates ranged from 97.2 to 106.0% for Bistoon milk and 93.16–102.5% for Kalleh milk. The optimized ZnS-CdS/Co nanoparticles showed low detection limits of 4.5 nM for CXM and 5.2 nM for TET. These findings underscore the potential of this rapid detection system as an effective tool for monitoring antibiotic residues in food products, significantly contributing to food safety and environmental sustainability. Future research could focus on enhancing the selectivity of these quantum dots for broader applications in complex matrices, promoting more sustainable antibiotic monitoring practices.

Keywords Nano-probe, Milk, Quantum dots, Fluorescence detection, Antibiotics

Quantum dots are semiconductor nanoparticles that exhibit unique optical and electronic properties due to their quantum confinement effect[1]. These nanoscale structures have gained significant attention in recent years for their potential applications in various fields, including sensing and detection[2,3]. One promising application of quantum dots is their use as sensors for identifying different compounds, including antibiotics, in a highly sensitive and specific manner[4].

The ability of quantum dots to emit fluorescent signals in response to specific stimuli makes them ideal candidates for sensor development. By functionalizing the surface of quantum dots with specific receptors or ligands, researchers can tailor their response to target molecules, enabling the detection of even trace amounts of analytes. This high sensitivity and selectivity make quantum dot sensors valuable tools for a wide range of applications, from environmental monitoring to medical diagnostics[5].

In the context of antibiotic detection, quantum dot sensors offer a rapid and reliable method for identifying the presence of these crucial compounds in various samples. With the increasing concern over antibiotic resistance and the need for effective monitoring of antibiotic use, the development of sensitive and selective detection methods is essential. Quantum dot sensors provide a promising solution to this challenge, offering a highly efficient means of detecting antibiotics in complex matrices[6].

[1]Department of Biology, Sanandaj Branch, Islamic Azad University, Sanandaj, Iran. [2]Department of Chemistry, Kermanshah Branch, Islamic Azad University, Kermanshah, Iran. ✉email: Fatemeh.Keshavarzi@iau.ac.ir

Overall, the unique properties of quantum dots make them powerful tools for sensing and detection applications, particularly in the identification of compounds such as antibiotics. With ongoing research and development efforts, quantum dot sensors are poised to revolutionize the field of analytical chemistry and contribute to advancements in various industries, from healthcare to environmental monitoring[7,8].

Fluorescence-based methods, such as fluorescence spectroscopy, have emerged as powerful tools for the identification of compounds due to their numerous advantages. One of the key benefits of fluorescence techniques is their ease of use, making them accessible to researchers and analysts across various fields. The instrumentation required for fluorescence spectroscopy is relatively simple and user-friendly, allowing for rapid and efficient analysis of samples. This simplicity in operation makes fluorescence-based methods a popular choice for routine analytical tasks, as they offer a straightforward and practical approach to compound identification[9].

In addition to being easy to use, fluorescence-based methods also offer high precision and accuracy in compound identification. The unique fluorescence properties of molecules enable sensitive detection and quantification, even at low concentrations. By measuring the emission of fluorescent signals from samples, researchers can obtain detailed information about the composition and characteristics of compounds present in the sample. This high level of precision and accuracy makes fluorescence spectroscopy a valuable tool for a wide range of applications, from pharmaceutical analysis to environmental monitoring. Overall, the combination of ease of use and high accuracy makes fluorescence-based methods indispensable for compound identification and analysis in diverse scientific disciplines[10].

CXM is a broad-spectrum antibiotic commonly used to treat a variety of bacterial infections in both humans and animals. However, the overuse or misuse of CXM can lead to adverse effects and the development of antibiotic resistance. It is crucial to accurately measure the levels of CXM in food products to prevent potential health risks associated with high doses of this antibiotic. Excessive consumption of CXM can result in allergic reactions, gastrointestinal disturbances, and the emergence of antibiotic-resistant bacteria, posing a significant threat to public health[11].

The precise measurement of CXM in food items is essential for ensuring food safety and preventing the potential negative consequences of antibiotic residue exposure. Regulatory agencies and food safety authorities must implement rigorous monitoring and control measures to detect and quantify CXM levels in food products. By employing accurate analytical methods for the detection of CXM residues, authorities can enforce strict guidelines on the use of this antibiotic in food production. This monitoring is critical for protecting consumers from the harmful effects of antibiotic residues and preserving the effectiveness of CXM for treating bacterial infections in both humans and animals[12,13].

TETs are a class of broad-spectrum antibiotics commonly used in both human and veterinary medicine to treat a variety of bacterial infections. They are also used in agriculture as growth promoters in livestock and poultry. However, the overuse and misuse of TETs can lead to their accumulation in food products and drinking water, posing potential health risks to humans and animals. High levels of TET in food and water can have adverse effects on human health, including allergic reactions, gastrointestinal disturbances, and antibiotic resistance. In animals, excessive exposure to TET can result in toxicity, reproductive issues, and the development of antibiotic-resistant bacteria[14].

Therefore, accurate identification and measurement of TET in food products and drinking water are crucial for monitoring and controlling their levels to ensure consumer safety and prevent the spread of antibiotic resistance[15–19]. Analytical techniques such as chromatography, mass spectrometry, and immunoassays are commonly used for the detection and quantification of TETs in various matrices. Regular monitoring and surveillance of TET residues in food and water sources are essential to assess the potential risks associated with their presence and to establish regulatory limits to protect public health and prevent environmental contamination[20].

While various methods have been reported for the measurement of CXM and TETs[21–24], the complexity and high cost associated with these methods have highlighted the need for a simple and cost-effective approach. Traditional analytical techniques such as chromatography and mass spectrometry offer high sensitivity and specificity but can be labor-intensive, time-consuming, and require expensive equipment. Immunoassays, while providing rapid results, may lack the desired sensitivity and specificity for accurate detection of CXM and TET. As a result, there is a growing demand for the development of a straightforward and affordable method that can reliably detect and quantify CXM and TET in food and water samples. Such a method would not only streamline the analysis process but also make monitoring TET residues more accessible and feasible for routine testing in various settings[25,26].

In summary, the introduction of Co-doped ZnS-CdS quantum dots as a fluorescence-based sensor for detecting CXM and TET marks a significant advancement in nanomaterial-based sensing technologies. This study provides a comprehensive characterization of the synthesized nanoparticles using scanning electron microscopy (SEM), photoluminescence (PL), energy dispersive X-ray (EDX), mapping, Line scan, Fourier-transform infrared spectroscopy (FT-IR) techniques, and X-ray diffraction (XRD), which offers crucial insights into their structural and optical properties. By harnessing the unique fluorescence characteristics of these quantum dots, our approach meets the pressing demand for straightforward, cost-effective, and sensitive methods to detect antibiotic residues in real samples. The promising applications of Co-doped ZnS-CdS quantum dots indicate a substantial improvement in accuracy and efficiency for antibiotic detection across various environmental and food safety contexts. Furthermore, we optimized the detection process through a systematic design of experiments (DOE) based on central composite design (CCD), which allowed for the refinement of critical parameters influencing fluorescence response. By establishing optimal conditions, we significantly enhanced the sensitivity and accuracy of CXM and TET detection at low concentrations. These optimized parameters not only streamline the measurement process but also ensure reliable results in practical applications, reinforcing

the potential of our approach to contribute to enhanced monitoring of antibiotic residues and improved food safety standards.

Experimental

Materials

Zinc nitrate hexahydrate ($Zn(NO_3)_2{\cdot}6H_2O$), cadmium acetate ($Cd(CH_3COO)_2$), cobalt nitrate hexahydrate ($Co(NO_3)_2{\cdot}6H_2O$), sodium sulfide (Na_2S), deionized water (DI), and ethanol are bought from Merck & Co. and utilized without undergoing purification processes. The pH of the environment was adjusted using a 0.1 M phosphoric acid and sodium phosphate solution, which was adjusted with 0.1 M hydrochloric acid and 0.1 M sodium hydroxide.

Preparation of Co-doped ZnS-CdS hybrid composite

Stage-1

For the synthesis of the ZnS-CdS hybrid composite, a standard protocol was followed. Initially, 0.2 mol of zinc nitrate was blended with 50 mL of a water–ethanol mixture in equal volumes (1:1), followed by the gradual addition of an equimolar amount of Na_2S solution. The resulting solution was magnetically stirred at 80 °C until a uniform milky white solution was achieved. The resulting powder was then subjected to centrifugation at 4000 rpm for 10 min and underwent two rounds of washing with distilled water, followed by another round of washing with ethanol to eliminate impurities before being dried in a hot air oven.

Stage-2

In the second phase of the process, a 0.1 mol concentration of cadmium acetate was combined with a 100 mL water–ethanol blend, followed by the addition of 0.1 mol Na_2S with ongoing agitation. Subsequently, 250 mg of ZnS powder and 0.1 mol of cobalt nitrate dopant were introduced into the aforementioned solution. Following 3 h of continuous stirring, the initially white solution transitioned to a white precipitate, signifying the formation of the ZnS-CdS composite. The resulting solution underwent centrifugation and multiple washes to eliminate impurities. To enhance the yield of the hybrid composite, the temperature was elevated to 120 °C and maintained for 120 min in a hot air oven.

Characterization techniques

The XRD patterns of the freshly synthesized hybrid composite were analyzed using the Shimadzu LABX XRD-6100 instrument. The Fourier-transform infrared (FT-IR) spectrum was obtained utilizing the Shimadzu IR Affinity-1S instrument, employing KBr pellets within the 400–4000 cm^{-1} range. Fluorescence emission intensity under 335 nm excitation was measured at room temperature using the Perkin-Elmer model LS45B. Furthermore, the surface morphology of Co-doped ZnS-CdS was studied using a scanning electron microscope (VEGA3).

The optimization of parameters by CCD

To optimize the five independent factors (pH, time, and temperature) within the experimental design, DOE was utilized based on the CCD method. The CCD method involves 2n axial runs, 2n factorial runs, and nc center runs (six replicates), where n represents the number of parameters. Given the direct correlation between these parameters and the response of the Co-doped ZnS-CdS sensor, and considering the synergistic effects among them, experimental conditions were optimized using a 20-point CCD. The experimental ranges considered were pH 5–8, time 10–60 min, and temperature 20–60 °C, encompassing a total of 20 experiments detailed in Table 1. A quadratic model was employed to analyze the three independent parameters through the mathematical relationship depicted in the subsequent equation.

$$\begin{aligned} Y = \beta_0 + (\beta_1 \times A) + (\beta_2 \times B) + (\beta_3 \times C) + (\beta_{11} \times A_2) + (\beta_{22} \times B_2) \\ + (\beta_{33} \times C_2) + (\beta_{12} \times AB) + (\beta_{13} \times AC) + (\beta_{23} \times BC) \end{aligned} \quad (1)$$

In Eq. (1) provided, Y represents the predicted response, and β0 denotes the model constant. The coefficients β_1, β_2, β_3, β_{11}, β_{22}, β_{33}, β_{12}, β_{13}, and β_{23} within the statistical model illustrate the linear, quadratic, and interactive effects of factors A (pH), B (Temperature), and C (Time) on the response, respectively. The CCD was conducted using Design-Expert software (Version 11.1.1.0 USA) to analyze the experimental data. Analysis of Variance

Factor	Name	Minimum	Maximum	Coded low	Coded high	Mean	Std. Dev.
CXM							
A	pH	3.98	9.02	−1 ↔ 5.00	+1 ↔ 8.00	6.50	1.27
B	Temperature	14.77	65.23	−1 ↔ 25.00	+1 ↔ 55.00	40.00	12.72
C	Time	0.6137	12.39	−1 ↔ 3.00	+1 ↔ 10.00	6.50	2.97
TET							
A	pH	2.64	9.36	−1 ↔ 4.00	+1 ↔ 8.00	6.00	1.70
B	Temperature	20.00	71.93	−1 ↔ 25.00	+1 ↔ 60.00	42.85	14.18
C	Time	0.6137	10.00	−1 ↔ 3.00	+1 ↔ 10.00	6.38	2.76

Table 1. Experimental parameters and levels in the 20 CCD for the optimization of pH, Temp, and Time.

(ANOVA) was carried out to assess the statistical significance at a 95% confidence interval with a p-value of 0.05. Additionally, regression analysis and response surface plotting were employed to determine the optimal conditions for evaluating the Co-doped ZnS-CdS sensor.

Selectivity

To explore the specificity and detectability of antibiotics, the presence of Co-doped ZnS-CdS as a sensor was investigated. A range of antibiotics including Ofloxacin, Amoxicillin, Azithromycin, Ceftriaxone, Ciprofloxacin, Clamoxin, Cotrimoxazole, TET, Metronidazole, Doxycycline, CXM, Rickettsia, Tetracim, Levofloxacin each at a concentration of 110.0 nM, were added to 10 µg of Co-doped ZnS-CdS. After thorough mixing for 10 min at room temperature and a pH of 7, the fluorescence intensity was measured upon excitation at 335 nm to assess the sensor's response to the presence of these antibiotics.

Detection of CXM and TET

Under carefully controlled conditions, varying doses of antibiotics such as CXM or TET were introduced to a composite material of Co-doped ZnS-CdS. The resulting fluorescence intensity at 580 nm, following excitation at 335 nm, was meticulously measured and documented. A calibration curve correlating F_0/F ratios (where F_0 denotes fluorescence intensity in the absence of antibiotics, and F corresponds to fluorescence intensity in the presence of different concentrations of CXM or TET) with the respective antibiotic concentrations was meticulously constructed. Subsequently, an in-depth evaluation of the selectivity of the Co-doped ZnS-CdS material was conducted, alongside the precise quantification of CXM or TET levels in authentic samples.

Preparation of real samples

Fresh samples of raw milk were obtained from local dairies Bistoon and Kalleh, sourced from a nearby supermarket. These samples were then subjected to a series of preparatory steps following the outlined methodology. In a standard procedure, 4 mL of raw milk was combined with 10 mL of water in a 50 mL beaker, followed by the addition of 2 mL of 10% trichloroacetic acid to the diluted mixture. The mixture was then subjected to sonication at 25 °C for 15 min and subsequently centrifuged at 10,000 rpm for 10 min to eliminate any sediment. The resulting supernatants were neutralized using a 30% NaOH solution and centrifuged at 20 °C for 10 min to ensure the removal of any remaining debris. Furthermore, for recovery experiments, real samples were intentionally spiked with CXM or TET, treated accordingly, and analyzed using the previously delineated procedure[22].

Results and discussion

In this section, we present the characterization results of the quantum dots (Co-doped ZnS-CdS). Once the structure of the Co-doped ZnS-CdS (ZnS-CdS/Co) was confirmed, it was used as a nano probe for the detection of CXM and TET. Important parameters such as temperature, time, pH, and the effect of different concentrations of CXM and TET were analyzed.

Characterization of Co-doped ZnS-CdS

In this section, we present the characterization results of the synthesized Co-doped ZnS-CdS nanomaterials, focusing on their structural and physical properties. SEM Analysis: SEM images were obtained to investigate the morphology and surface characteristics of the ZnS-CdS/Co. The SEM analysis revealed uniform and spherical nanoparticles with an average size of approximately 2–5 nm. The images also indicated a high degree of dispersion and minimal aggregation, suggesting the successful synthesis of well-defined quantum dots (Fig. 1A). Additionally, Fig. 1B corresponds to the elemental mapping, illustrating the distribution of elements and their densities on the nanoparticle's surface. As depicted in Fig. 1B, the highest density corresponds to the Cd element, represented by the color green.

Figure 1C, which is the EDX of ZnS-CdS/Co, shows the elements and their percentage in the nanoparticle. According to Fig. 1C, the highest percentage is attributed to cadmium, accounting for 60.9%, and various elements such as Zn, S and Co are also present in the structure.

Another technique utilized is line scanning, as depicted in Fig. 1D, to illustrate the distribution of surface elements effectively. Each color in the image corresponds to a particular element present in the sample; for instance, pale green indicates cadmium (Cd La1), orange represents zinc (Zn Ka1,2), blue signifies sulfur (S Ka1,2), red signifies cobalt (Co Ka1) and so forth, demonstrating the diverse elemental composition within the structure.

FT-IR spectroscopy was used to analyze the chemical bonds and functional groups of the as-prepared hybrid composite. Figure 2A shows the FT-IR spectrum of the Co-doped ZnS-CdS hybrid composite. The band at 423 cm^{-1} is attributed to the metal sulfide bond (Cd–S). Similarly, the bands at 518 cm^{-1} and 621 cm^{-1} are related to the metallic bond of Zn–S, corresponding to the stretching of zinc and sulfide. The band at 1128 cm^{-1} is attributed to the –OH mode of the water molecule. The band at 1619 cm^{-1} corresponds to the stretching vibration mode of O–H, and the band at 2309 cm^{-1} corresponds to the –O–C–O stretching mode. The bands at 3432 cm^{-1} and 3726 cm^{-1} correspond to surface-absorbed water. Additional bands at 848 cm^{-1} and 944 cm^{-1} specify the individual resonance interface among the vibrational modes of sulfide ions in the crystal[27,28].

The XRD analysis was performed to assess the crystallinity and phase composition of the newly synthesized Co-doped ZnS-CdS hybrid composite. Figure 2B illustrates the XRD patterns of the composite, revealing distinct peaks at angles $2\theta = 29.6°$, 34.7°, 46.7°, 56.7°, and 58.9°, which can be attributed to ZnS and are consistent with the cubic structure of ZnS (JCPDS card number: 05–0566, with lattice parameter a = 0.54506 nm). Additionally, prominent peaks at angles $2\theta = 27.7°$, 31.7°, and 54.4° correspond to CdS and align with the cubic structure of CdS (JCPDS card number: 80-0019, with lattice parameter a = 0.5648 nm). Importantly, no significant diffraction

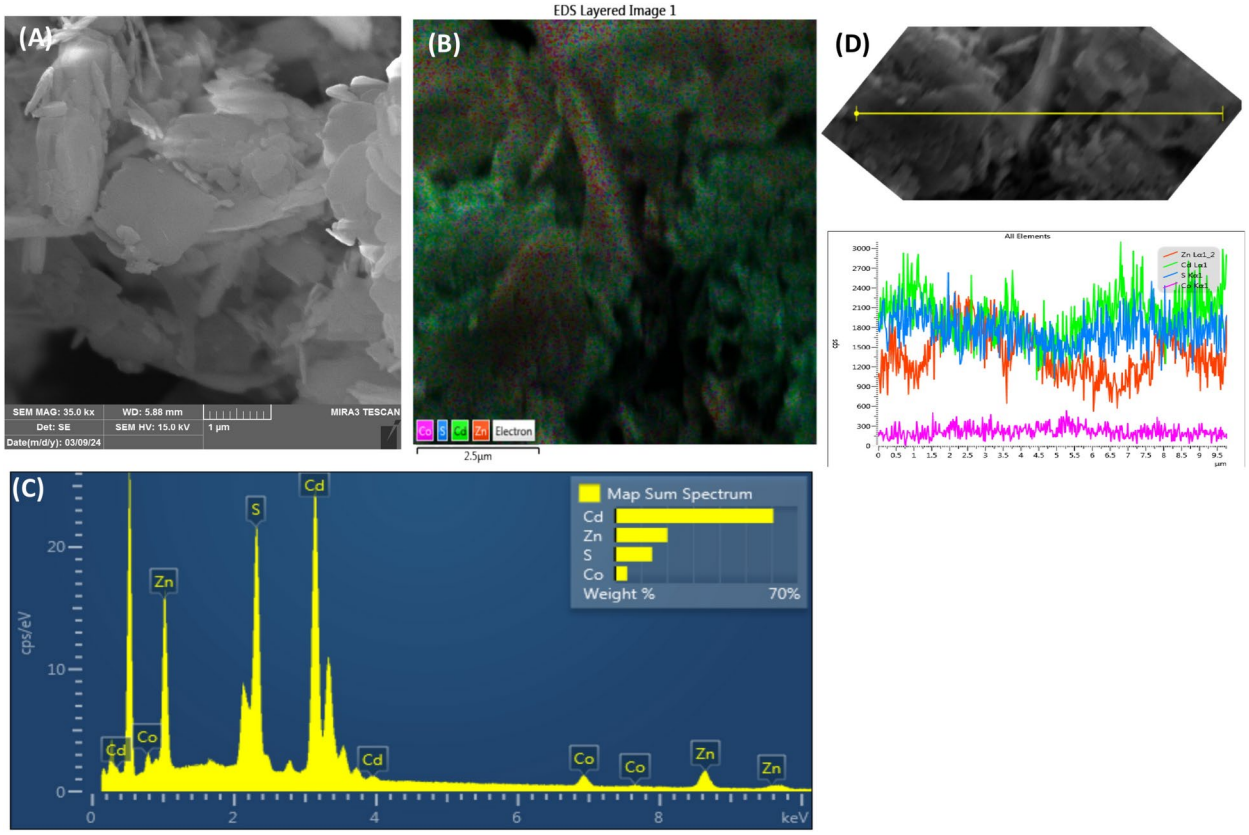

Fig. 1. (**A**) SEM images of ZnS-CdS/Co, (**B**) mapping imaging of ZnS-CdS/Co, (**C**) EDS of ZnS-CdS/Co, (**D**) Line scan analysis of the ZnS-CdS/Co hybrid composite. The colored mapping in the image illustrates the distribution of various elements pale green indicates cadmium (Cd La1), orange represents zinc (Zn Ka1,2), blue signifies sulfur (S Ka1,2), and red denotes cobalt (Co Ka1).

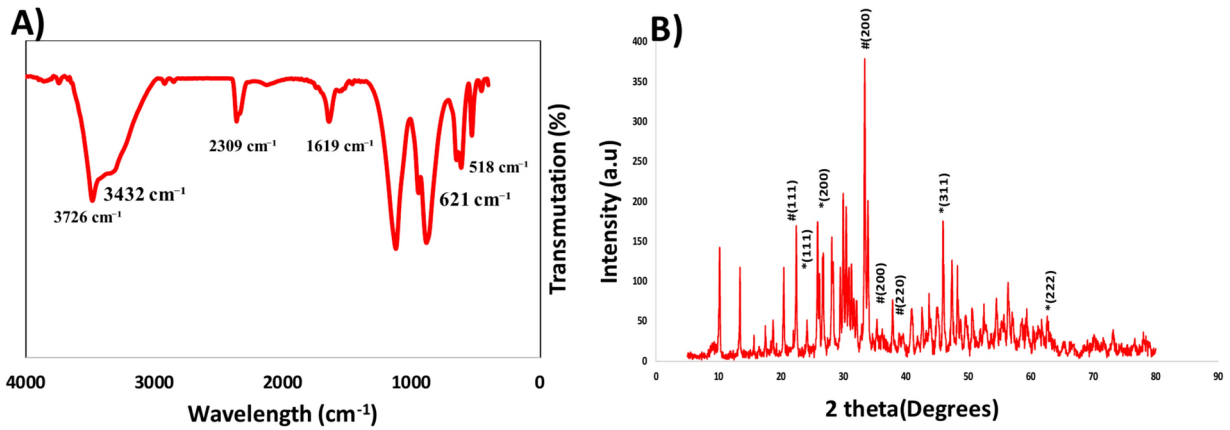

Fig. 2. (**A**) FTIR spectra of ZnS-CdS/Co, (**B**) XRD pattern of ZnS-CdS/Co hybrid composite.

patterns indicative of other phases or impurities were observed, indicating the successful incorporation of Co dopant ions into the host lattice. This underscores the achievement of a highly pure ZnS-CdS structure through the synthesis process[29].

Optical properties of ZnS-CdS/Co

This subsection analyzes the optical properties of ZnS-CdS/Co nanoparticles, including their light absorption and emission characteristics. The fluorescence composition of this compound was investigated and studied under excitation with different wavelengths ranging from 240 to 350 nm. For excitation with a wavelength of

220–330 nm, all peaks are broad and none are sharp. However, at higher excitation levels, the peaks become sharper and have the highest intensity of fluorescence emission. This is seen in the peak where the excitation was placed at 335 nm. It was observed that at a wavelength of 335 nm, the peak has a suitable height and is not too wide. Therefore, the best case for ZnS-CdS/Co is excitation at 335 nm. The intensity of the emission spectrum of ZnS-CdS/Co is extremely high due to the presence of different atoms in the structure (Fig. 3).

Response of ZnS-CdS/Co

Here, we discuss the response behavior of the ZnS-CdS/Co nanoprobe under varying experimental conditions (such as temperature, time, and pH), assessing its performance. Due to the presence of different elements in the structure of ZnS-CdS/Co that can interact differently with biological compounds, experiments were conducted by adding various compounds, including Ofloxacin, Amoxicillin, Azithromycin, Ceftriaxone, Ciprofloxacin, Clamoxin, Cotrimoxazole, TET, Metronidazole, Doxycycline, CXM, Rickettsia, Tetracim, Levofloxacin, and recording changes in their fluorescence spectra. It was observed that significant changes occurred only in the presence of CXM and TET. Specifically, as the concentration of CXM and TET increased in the presence of ZnS-CdS/Co, there was a notable decrease in fluorescence intensity. However, for the other substances or changes, the observed fluorescence changes were either very low or negligible, to the extent that they could be disregarded. This indicates that ZnS-CdS/Co dots selectively interact with aqueous solutions to detect CXM and TET, as illustrated in Fig. 4.

Statistical analysis

This part provides a statistical analysis of the data collected to establish the reliability and significance of our measurement results. A total of 20 experiments were designed using the CCD model to investigate the parameters, with the corresponding responses displayed in Table 2 for CXM and Table 3 for TET. The responses, represented by fluorescence intensity (F_0/F), ranged from 0.9 to 1.5 (F_0/F) for CXM and from 0.9 to 3.5 for TET. The CCD model has the advantage of capturing complex response functions with a minimal number of variable combinations. In practice, 20 runs were performed for each F_0/F to consider the quadratic equation for both CXM and TET. The summary statistics of the proposed model are presented in Table 4, which were fitted to a quadratic equation with a high adjusted R-squared (Adj R2) value. Multiple regression analysis techniques were employed to determine the quadratic model coefficients in the Response Surface Methodology (RSM). The resulting quadratic model for the response was expressed in terms of coded factors, as described by the following equation:

$$Y = 1.30 + (0.0444 \times A) + (0.0037 \times B) + (0.1141 \times C) - (0.0373 \times A_2) - (0.0020 \times B_2) - (0.0285 \times C_2) + (0.0062 \times AB) + (0.0162 \times AC) - (0.0063 \times BC) \quad (2)$$

$$Y = 3.93 + (0.5761 \times A) + (0.0300 \times B) + (0.7459 \times C) - (0.5021 \times A_2) - (0.1465 \times B_2) - (0.7607 \times C_2) + (0.0000 \times AB) + (0.2000 \times AC) - (0.0000 \times BC) \quad (3)$$

the negative and positive signs illustrate an opposite and a synergistic effect, respectively.

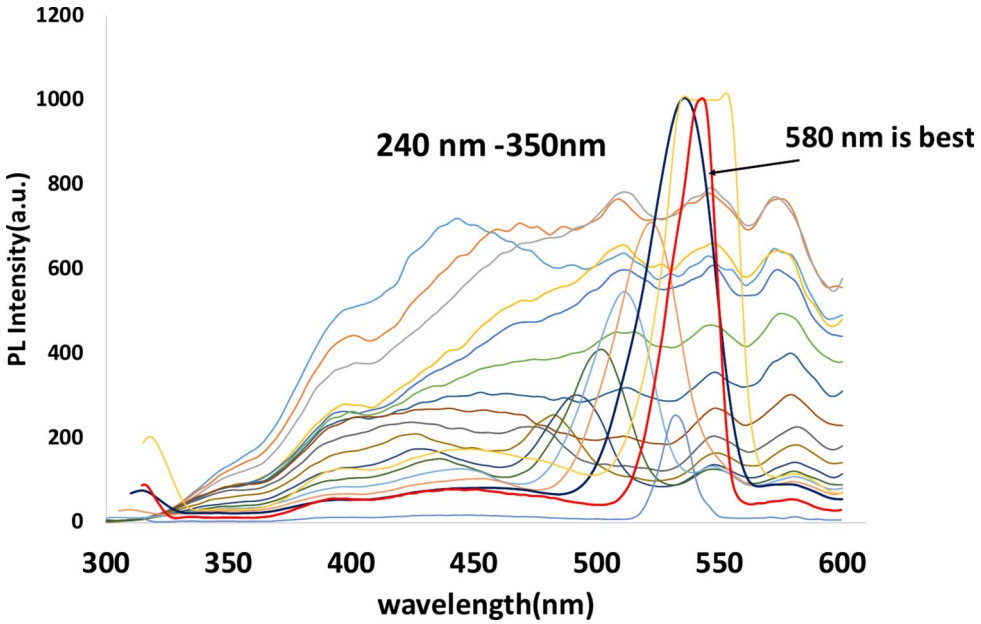

Fig. 3. The fluorescence spectrum of (ZnS-CdS/Co) in excitation with different wavelengths from 240 to 360 nm.

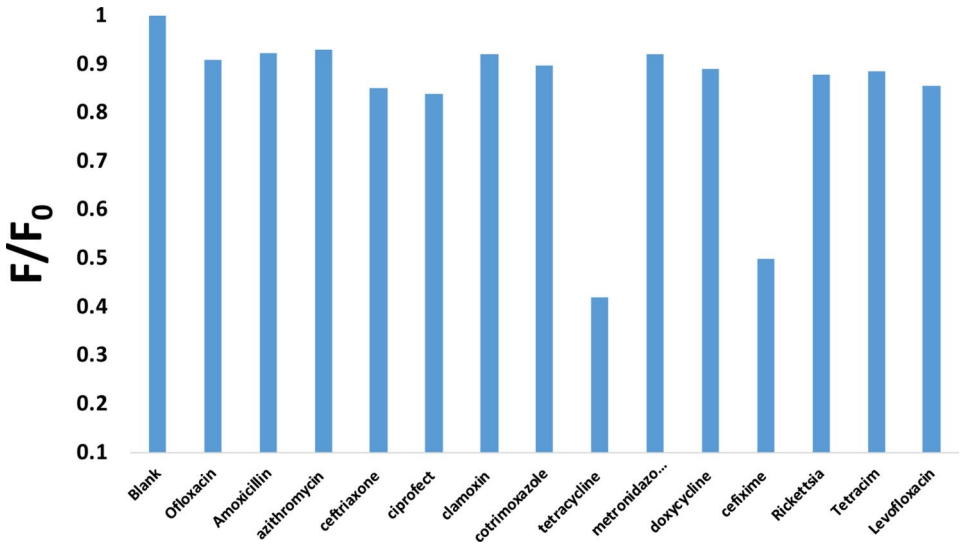

Fig. 4. Response of ZnS-CdS/Co with biological compounds.

Std	Run	Factor 1 A: pH	Factor 2 B: Temperature °C	Factor 3 C: Time min	Response 1 R1 F0/F
17	1	6.5	40	6.5	1.3
3	2	5	55	3	1.09
16	3	6.5	40	6.5	1.3
18	4	6.5	40	6.5	1.3
6	5	8	25	10	1.4
12	6	6.5	65.2269	6.5	1.3
9	7	3.97731	40	6.5	1.1
15	8	6.5	40	6.5	1.3
19	9	6.5	40	6.5	1.3
2	10	8	25	3	1.1
14	11	6.5	40	12.3863	1.4
8	12	8	55	10	1.4
4	13	8	55	3	1.15
11	14	6.5	14.7731	6.5	1.3
10	15	9.02269	40	6.5	1.3
20	16	6.5	40	6.5	1.3
5	17	5	25	10	1.3
13	18	6.5	40	0.613725	1.05
7	19	5	55	10	1.3
1	20	5	25	3	1.09

Table 2. Experiment runs and responses for optimizing parameters evaluation (CXM).

ANOVA

The aim here is to apply ANOVA (Analysis of Variance) to compare significant differences among various groups within our obtained data. ANOVA was carried out for the quadratic model represented in Eq. (2) for CXM and Eq. (3) for TET regarding the F_0/F, as detailed in Table 5 for CXM and Table 6 for TET. A low p-value in Fisher's statistic indicates the regression model's high significance. Significance of the regression coefficients for the variables can be evaluated using a T-test. Additionally, the interactions among different parameters can be inferred from the p-values. A coefficient is considered significant if the t-value is large and the corresponding p-value is small. The ANOVA test indicated the model's significance due to a p-value below 0.05. Model terms are deemed significant if the probability > F is less than 0.05 based on the p-values.

Accordingly, in this case A, C, AC, A^2, C^2 are significant model terms for CXM and A, C, A^2, C^2 are significant model terms for TET in Eqs. (2 and 3) to show the single and concerning results of the three investigated parameters on the F_0/F. Therefore, the insignificant term is not seen in this model, and this model was presented

Std	Run	Factor 1	Factor 2	Factor 3	Response 1
			B: Temperature	C: Time	R1
		A: pH	°C	min	F0/F
4	1	8	60	3	1.8
14	2	6	42.5	10	3.9
13	3	6	42.5	0.613725	1.01
10	4	9.36359	42.5	6.5	3.9
18	5	6	42.5	6.5	3.9
5	6	4	25	10	2.5
19	7	6	42.5	6.5	3.9
2	8	8	25	3	1.8
20	9	6	42.5	6.5	3.9
9	10	2.63641	42.5	6.5	1.6
3	11	4	60	3	1.2
11	12	6	20	6.5	3.9
1	13	4	25	3	1.2
16	14	6	42.5	6.5	3.9
8	15	8	60	10	3.9
12	16	6	71.9314	6.5	3.9
6	17	8	25	10	3.9
7	18	4	60	10	2.5
17	19	6	42.5	6.5	3.9
15	20	6	42.5	6.5	3.9

Table 3. Experiment runs and responses for optimizing parameters evaluation (TET).

Source	Sequential p-value	Adjusted R^2	Predicted R^2	
CXM				
Linear	< 0.0001	0.8231	0.7646	
2FI	0.7844	0.7988	0.6158	
Quadratic	**< 0.0001**	**0.9693**	**0.8752**	**Suggested**
Cubic	0.0014	0.9963	0.7430	Aliased
TET				
Linear	0.0023	0.5068	0.3445	
2FI	0.9374	0.4114	− 0.7294	
Quadratic	**< 0.0001**	**0.9277**	**0.6329**	**Suggested**
Cubic		1.0000		Aliased

Table 4. Model summary statistic. Significant values are in bold.

based on the insignificant terms by Eqs. (4 and 5). The predicted response value of the F_0/F based on Eq. (3) is presented in Table 5 for CXM and Table 6 for TET. The regression coefficient value of Eqs. (4 and 5) is ($R^2 = 0.9693$) for CXM and ($R^2 = 0.9619$) for TET (Table 7). As shown in Table 7, the mean square because of the residual error and the ratio of the mean square owing to the regression can be acquired from the ANOVA test, which is used to predict the statistical significance of these terms. It is evident that with a p-value less than 0.001, the F values of this model were higher, suggesting that the response can be satisfactorily elucidated by its corresponding model equation. Overall, a p-value less than 0.001 indicates a 99% confidence interval and significance at the 0.01 level for the model[30]. As seen in Table 5 and 6, the linear effects of the parameters A ($p < 0.0001$), B ($p = 0.7466$), and C ($p < 0.0001$) for TET and A ($p < 0.0001$), B ($p = 0.5085$), and C ($p < 0.0001$) for CXM on the responses were statistically significant, and the variables of A and C were shown to be extremely significant. Also, the squared terms of A^2 ($p < 0.0001$) for TET and C^2 ($p < 0.0001$) for CXM were extremely significant. All of the terms related to the interaction effects were also significant. The actual quadratic equation of the response based on the actual variables is given using Eq. (6) for CXM and Eq. (7) for TET.

$$Y = 1.30 + (0.0444 \times A) + (0.0037 \times B) + (0.1141 \times C) - (0.0373 \times A_2) - (0.0020 \times B_2) - (0.0285 \times C_2) + (0.0062 \times AB) + (0.0162 \times AC) - (0.0063 \times BC) \quad (4)$$

Source	Sum of squares	df	Mean square	F-value	p-value	
Model	0.2370	9	0.0263	67.64	< 0.0001	Significant
A-pH	0.0269	1	0.0269	69.16	< 0.0001	
B-temperature	0.0002	1	0.0002	0.4702	0.5085	
C-time	0.1779	1	0.1779	456.94	< 0.0001	
AB	0.0003	1	0.0003	0.8027	0.3913	
AC	0.0021	1	0.0021	5.43	0.0421	
BC	0.0003	1	0.0003	0.8027	0.3913	
A^2	0.0201	1	0.0201	51.60	< 0.0001	
B^2	0.0001	1	0.0001	0.1450	0.7113	
C^2	0.0117	1	0.0117	30.06	0.0003	
Residual	0.0039	10	0.0004			
Lack of fit	0.0039	5	0.0008			
Pure error	0.0000	5	0.0000			
Cor total	0.2409	19				

Table 5. ANOVA for response surface quadratic model for F0/F(CXM).

Source	Sum of squares	df	Mean square	F-value	p-value	
Model	24.52	9	2.72	28.07	< 0.0001	Significant
A-pH	4.53	1	4.53	46.71	< 0.0001	
B-Temperature	0.0107	1	0.0107	0.1104	0.7466	
C-Time	5.91	1	5.91	60.91	< 0.0001	
AB	0.0000	1	0.0000	0.0000	1.0000	
AC	0.3200	1	0.3200	3.30	0.0995	
BC	0.0000	1	0.0000	0.0000	1.0000	
A^2	3.69	1	3.69	38.00	0.0001	
B^2	0.2231	1	0.2231	2.30	0.1605	
C^2	5.20	1	5.20	53.60	< 0.0001	
Residual	0.9705	10	0.0971			
Lack of fit	0.9705	5	0.1941			
Pure error	0.0000	5	0.0000			
Cor total	25.49	19				

Table 6. ANOVA for response surface quadratic model for F0/F(TET).

CXM			
Std. Dev.	0.0197	R^2	0.9838
Mean	1.25	Adjusted R^2	0.9693
C.V. %	1.57	Predicted R^2	0.8752
		Adeq Precision	27.5150
TET			
Std. Dev.	0.3115	R^2	0.9619
Mean	3.02	Adjusted R^2	0.9277
C.V. %	10.31	Predicted R^2	0.6329
		Adeq Precision	16.1094

Table 7. Standard deviation and R^2 of the response.

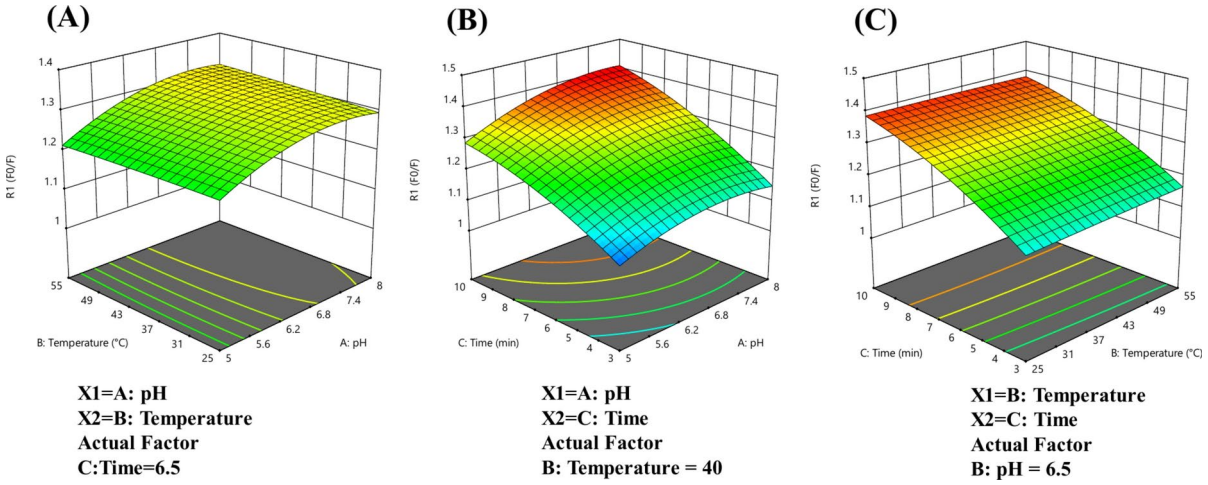

Fig. 5. The 3D plot for interaction effects between pH and temperature at 6.5 min on F_0/F (**A**), pH and time at 40 °C on F_0/F (**B**) and temperature and time at pH = 6.5 (**C**) on F_0/F for the response surface quadratic model.

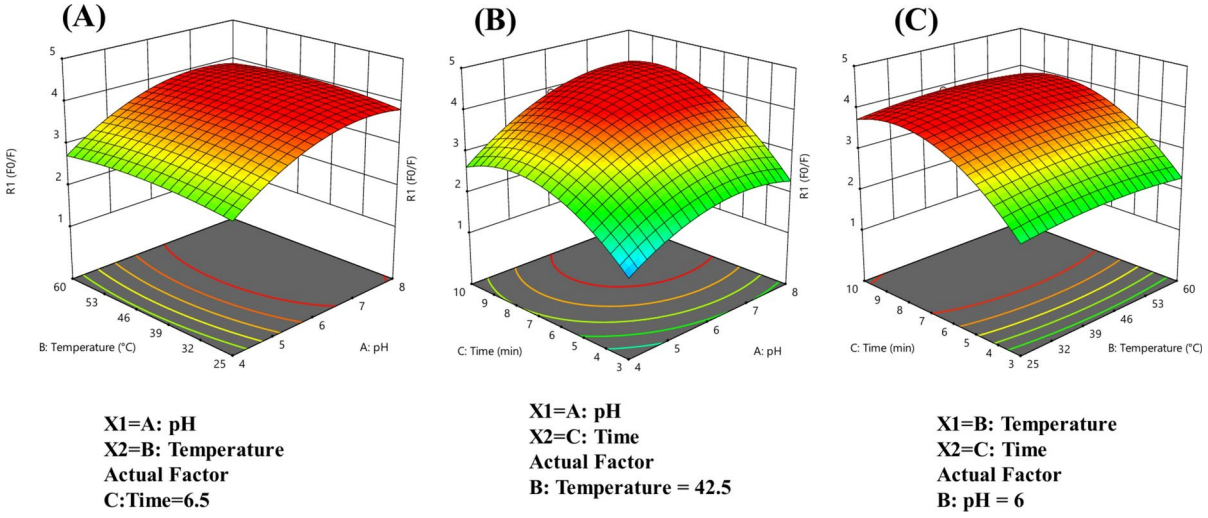

Fig. 6. The 3D plot for interaction effects between pH and temperature at 6.5 min on F_0/F (**A**), pH and time at 42.5 °C on F_0/F (**B**) and temperature and time at pH = 6 (**C**) on F_0/F for the response surface quadratic model.

$$Y = 3.93 + (0.5761 \times A) + (0.0300 \times B) + (0.7459 \times C) - (0.5021 \times A_2) - (0.1465 \times B_2) - (0.7607 \times C_2) + (0.0000 \times AB) + (0.2000 \times AC) - (0.0000 \times BC) \quad (5)$$

$$Y = 0.2448 + (0.2140 \times A) + (0.000048 \times B) + (0.04749 \times C) - (0.0165 \times A_2) - (0.0000086 \times B_2) - (0.0023 \times C_2) + (0.00027 \times AB) + (0.0030 \times AC) - (0.000119 \times BC) \quad (6)$$

$$Y = -6.1496 + (1.6084 \times A) + (0.0423 \times B) + (0.8489 \times C) - (0.1255 \times A_2) - (0.00047 \times B_2) - (0.0621 \times C_2) + (0.0000 \times AB) + (0.0285 \times AC) - (0.0000 \times BC) \quad (7)$$

3D response surface plots

The different outcomes associated with the parameters and their interaction effects on the response can be elucidated through the analysis of 3D response surface plots. These plots visually represent how the response of the Co-doped ZnS-CdS sensor reaches maximum or minimum values within specific parameter ranges. Notably, a specific region exists where the peak current remains constant, neither decreasing nor increasing. This observation aligns with the identification of optimal parameter settings required to enhance the Co-doped ZnS-CdS sensor response. This result corroborated desirable levels of parameters to increase the sensor response.

From Figs. 5 and 6, as well as Tables 5 and 6 for CXM and TET, it is evident that there is a significant interaction between parameters A (pH) and B (temperature) in the response (F0/F). Parameter B (temperature) has minimal impact on the response. Furthermore, Tables 5 and 6 show that the square terms A^2 for CXM and C^2

for TET were significant. The curved lines in Figs. 5B and 6B demonstrate fluctuations in response by enhancing the pH and time. Moreover, there are notable interactions between A (pH) and C (time) (Figs. 5B,6B). In Tables 5 and 6, the term AC confirms these interactions. For the diagram BC (Figs. 5C, 6C), it is similar to AB, because the temperature does not have much of an effect and the intensity of F0/F increases with the increase of time. The optimization was performed by keeping parameters A (pH), B (temperature), and C (time) within specified ranges, while the responses were changed to reach the optimal response. Parameters A, B, and C were varied within the ranges of 4–8, 25–60 °C, and 3–10 min, respectively. The fluorescence intensity was maximized at A = 6.00, B = 42.5, and C = 6.5 for TET and A = 6.50, B = 40.0, and C = 6.5 for CXM.

Detection of TET

The high fluorescence intensity of ZnS-CdS/Co, especially in the presence of TET showed a significant change. Therefore, ZnS-CdS/Co can be used as a sensor for detecting TET. To study the sensitivity of the ZnS-CdS/Co composition to TET, various concentrations of TET were added to the ZnS-CdS/Co in an aqueous medium and its fluorescence intensity was measured at a wavelength of 580 nm under optimal conditions (Fig. 7A). Upon adding TET to the ZnS-CdS/Co across a wide concentration range from 7 to 900 nM, a consistent decrease in fluorescence intensity was observed. Plotting the ratio of TET concentration to F0/F, where F0 represents the fluorescence intensity without TET and F represents the intensity in the presence of varying TET concentrations, yielded a highly linear graph with an R-value of 96.23% in the range of 0–220 nM (Fig. 7B) and 96.86% in the range of 220–900 nM (Fig. 7C). The method demonstrated a low detection limit of 5.24 nM with a signal-to-noise ratio of 3.

Detection of CXM

The ZnS-CdS/Co exhibited high fluorescence intensity, with a noticeable change in the presence of CXM, suggesting its potential as a sensor for detecting CXM. To assess the sensitivity of ZnS-CdS/Co to CXM, various concentrations of CXM were introduced to the ZnS-CdS/Co in an aqueous solution, and the fluorescence intensity was measured at 580 nm under optimal conditions (Fig. 8A). A consistent reduction in fluorescence intensity was observed as CXM was added across a broad concentration range of 6–1200 nM. The plot of CXM concentration against F_0/F ratio, where F_0 represents the fluorescence intensity in the absence of CXM and F represents the intensity with varying CXM concentrations, resulted in a highly linear graph with an R-value of 9056% in rang (0–120 nM) (Fig. 8B) and 91.77% in rang (120–1200 nM) (Fig. 8C). This method exhibited a low detection limit of 4.5 nM with a signal-to-noise ratio of 3.

Interference study

In this section, we will explore any potential interfering effects from other substances that may affect the detection capabilities of our nanoprobe. The selectivity of the ZnS-CdS/Co in measuring CXM and TET was examined by studying the effects of electrolytes and biological samples including amino acids, ions (Ca^{2+}, Mg^{2+}, Zn^{2+}, Na^{+}, K^{+}, Cl^{-}), and proteins. The results are reported in Fig. 9. When CXM and TET are alone in the environment,

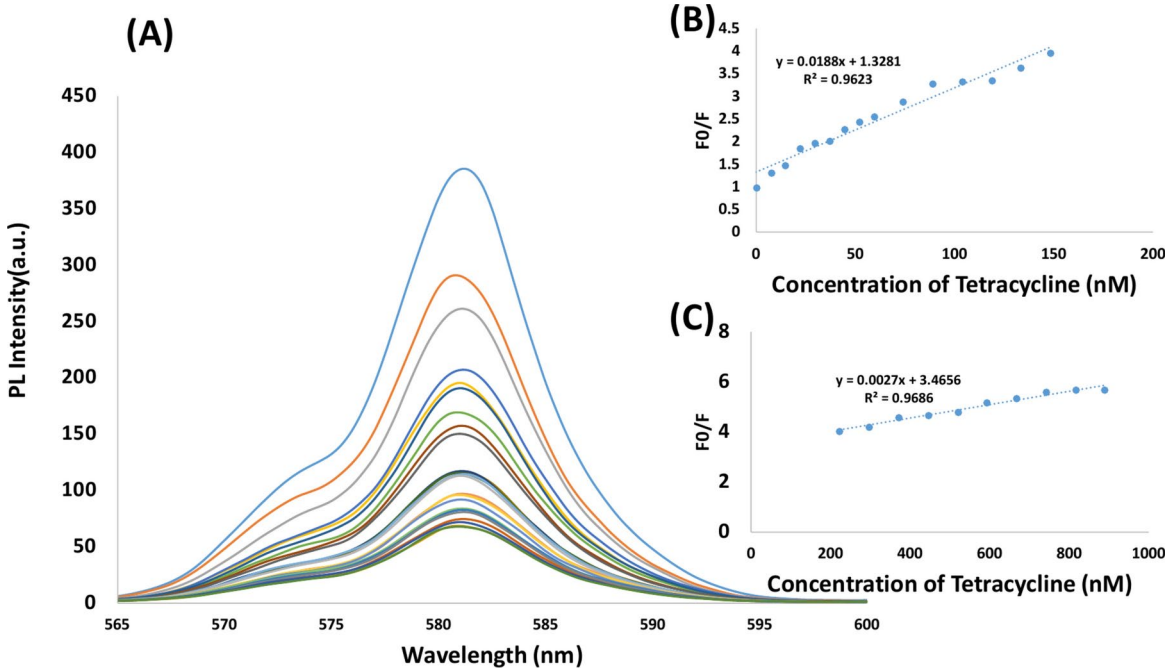

Fig. 7. (**A**) The fluorescence diagram of ZnS-CdS/Co sensor in the presence of TET at concentrations ranging from 6.0 nM to 900.0 nM. (**B**) F_0/F ratio of ZnS-CdS/Co at TET concentrations ranging from 0 nM to 220 nM. (**C**) F_0/F ratio of ZnS-CdS/Co atTET concentrations ranging from 220 nM to 900 nM.

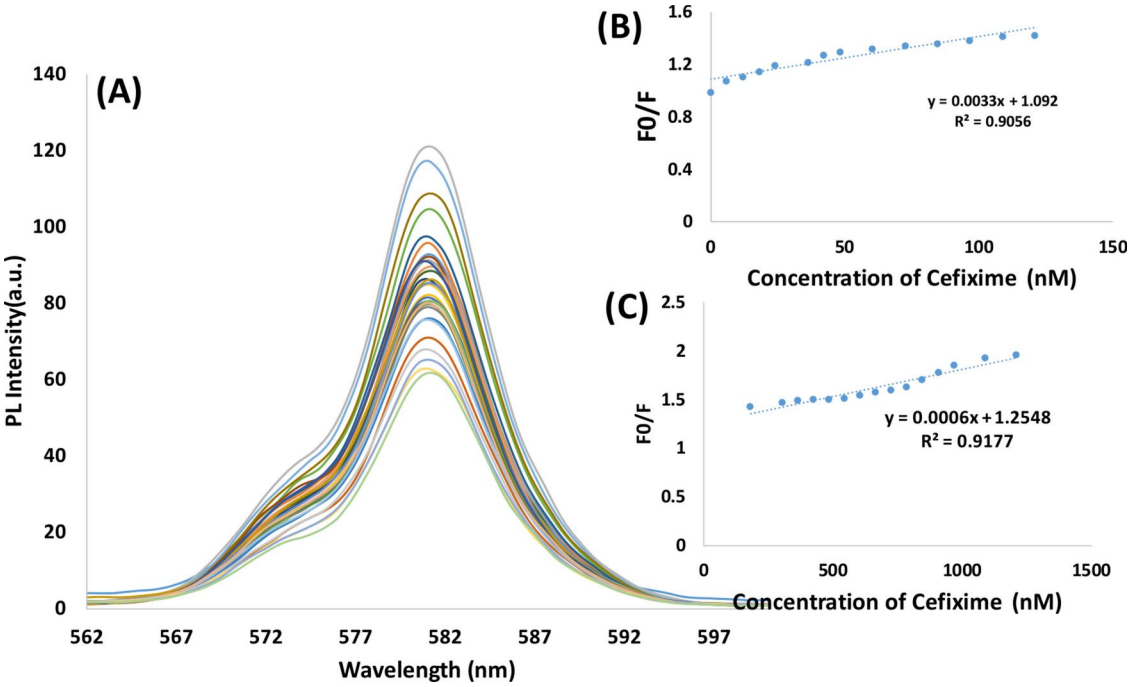

Fig. 8. (**A**) The fluorescence diagram of ZnS-CdS/Co sensor in the presence of CXM at concentrations ranging from 7.0 nM to 1200.0 nM. (**B**) F_0/F ratio of ZnS-CdS/Co at CXM concentrations ranging from 0 nM to 120 nM. (**C**) F_0/F ratio of ZnS-CdS/Co at CXM concentrations ranging from 120 nM to 1200 nM.

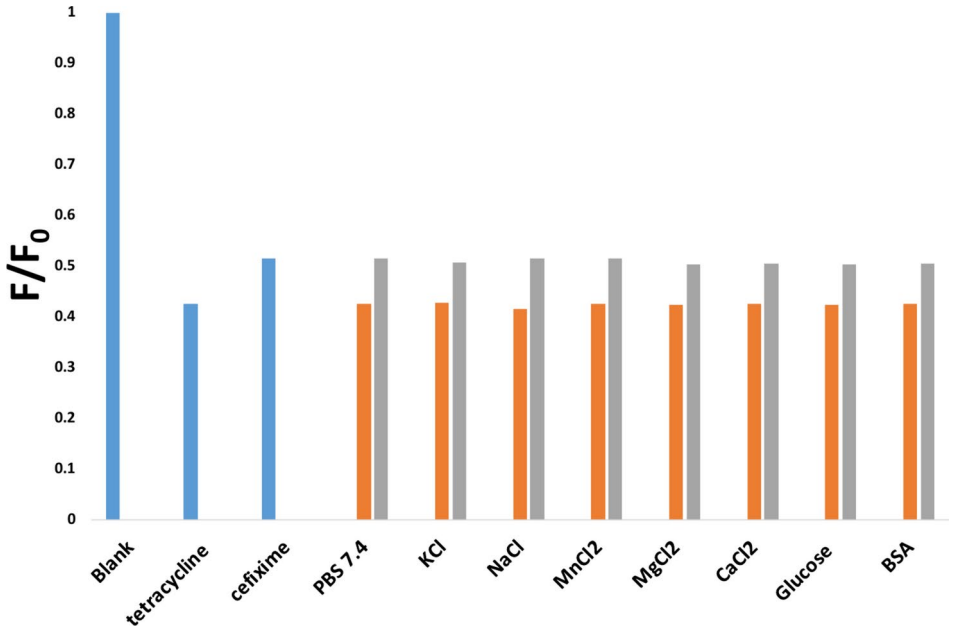

Fig. 9. The selectivity of the ZnS-CdS/Co in the determination of CXM and TET.

changes in F/F_0 are insignificant compared to when they are with other compounds. This indicates that the other compounds mentioned in the test do not affect the detection of CXM and TET.

Application in determination of CXM and TET in real samples

Finally, this section investigates practical applications for detecting CXM and TET in real samples, demonstrating the feasibility and effectiveness of our proposed technique. For the first time, the quantitative detection of CXM and TET in milk samples from two different sources (local dairies Bistoon and Kalleh) was investigated at three distinct concentrations (Table 8). The recovery rates for CXM in spiked milk samples varied from 96.0 to

Local dairies (Milk)	Added (μM)	Found (nM)	Recovery (%)	RSD%
CXM				
Bistoon	10.0	9.6	96.0	1.5
	50.0	50.06	100.12	1.26
	90.0	90.7	100.77	0.87
Kalleh	10.0	10.5	100.5	1.8
	50.0	48.5	97.0	2.5
	90.0	90.3	100.33	0.95
TET				
Bistoon	5.0	4.8	97.2	2.5
	20.0	20.5	102.5	1.32
	50.0	50.12	100.24	3.2
Kalleh	5.0	5.3	106.0	1.9
	20.0	19.2	96.0	2.5
	50.0	46.58	93.16	2.8

Table 8. Determination of CXM and TET concentration in real samples. By fluorescence method (n = 5).

Probe	Linear range	LOD	Antibiotics	Real sample	[Refs.]
MoS and CdTe quantum dots	0.1–1 μM	–	TET	Milk	[24]
Zinc-doped carbon quantum dots	0.1–50 μM	61.1 nM	TET	Tap water, river water, milk, eggs, and chicken	[31]
S, N-doped carbon quantum dots	1.88–60 μmol/L	0.56 μmol/L	TET	Milk and honey	[32]
$CsPbBr_3$ quantum dot-based	0.2–5.0 μM	28 nM	TET	Aqueous phase	[33]
Tungsten disulfide	200–2.500 ng/mL	45 ng/mL	CXM	Milk	[34]
Nanocomposite optosensor of dual quantum dot	10–50.0 μg/L	0.10 μg/L	CXM	Milk	[35]
Fe_3O_4@SiO_2 modified graphene oxide	0.001–0.7 μg/mL	0.54 ng mL^{-1}	CXM	Urine samples	[36]
Nitrogen-doped carbon quantum	0–100.0 μM	0.344 μM	TET	Rat serum and milk	[37]
ZnS quantum	200–6000 nM	30 pM	TET	Food products of animal origin	[38]
ZnS-CdS/Co	7.0–900.0 nM	5.2 nM	TET	Milk	This work
ZnS-CdS/Co	6.0–1200.0 nM	4.5 nM	CXM	Milk	This work

Table 9. Comparison of the performances of various ZnS-CdS/Co for detection of CXM and TET. *LOD* Limit of detection.

100.77% for the Bistoon milk and from 100.5 to 100.33% for the Kalleh milk. Similarly, the recovery rates for TET ranged from 97.2 to 106.0% for Bistoon milk and from 93.16 to 102.5% for Kalleh. These results indicate a promising reliability of the proposed analytical method. However, to strengthen our findings, further analysis of additional samples from various locations and comparison with established reference procedures are warranted.

Performance of the quantum dots probe utilized for the detection of CXM and TET was assessed in comparison with another constructed probe, and the findings are presented in Table 9. The proposed probe demonstrated a significantly lower detection limit compared to the values obtained by the alternative probe, attributable to the heightened sensitivity of ZnS-CdS/Co[24,31–38].

Reaction mechanism

The selective detection of CXM and TET by the ZnS-CdS/Co composite sensor is primarily influenced by the unique surface properties of the composite, which enhance interactions with specific functional groups present in these antibiotics. CXM features amine, carboxyl, and ether groups, while TET contains hydroxyl and ketone groups. These functional groups engage in various interactions, such as hydrogen bonding and π–π stacking, with the sensor's surface, leading to changes in the local electronic environment. This interaction alters the electrochemical behavior of the composite, resulting in a measurable change in the sensor's signal, whether it be through quenching or enhancement of PL and conductivity. Additionally, band gap engineering plays a crucial role in optimizing the electronic properties of the ZnS and CdS components, allowing for the effective targeting of the antibiotics' unique redox behavior. By tuning the band gap, the composite can facilitate optimal electron transfer during the sensing process, as the energy levels align with those of the antibiotics. This compatibility enhances the interaction between the sensor and the analytes, generating distinct electrochemical signatures corresponding to each antibiotic. Overall, these mechanisms enable the ZnS-CdS/Co composite to selectively and sensitively detect CXM and TET, even in complex mixtures[6,8].

Conclusions

Excessive use of antibiotics such as TET and CXM poses significant risks to human health and the environment. Thus, there is an urgent need to develop sensitive and efficient methods to detect and quantify these antibiotics in environmental samples. Fluorescence spectroscopy emerges as a powerful tool for identifying biomolecules due to its high sensitivity and cost-effectiveness. Leveraging this technique could allow researchers to establish reliable methods for detecting TET and CXM. This work demonstrates, for the first time, the usefulness of affordable ZnS-CdS/Co in developing highly fluorescent quantum dots with substantial potential as sensors. The results indicated high fluorescence intensity with a narrow size distribution (average particle size: 2–5 nm), showcasing good performance across various concentrations: 7.0–900.0 nM for TET and 6.0–1200.0 nM for CXM using ZnS-CdS/Co as probes with acceptable recovery percentages. Furthermore, our ZnS-CdS/Co nanoparticles exhibited outstanding performance in accurately determining low concentrations of CXM (LOD of 4.5 nM) and TET (LOD of 5.2 nM). The probe was optimized to meet essential analytical requirements including cost efficiency, good recovery percentage, and adaptability to real sample sources through a mix-and-read analytical strategy. Looking ahead, future studies could explore enhancing the selectivity of ZnS-CdS/Co probes by functionalizing them with specific ligands or antibodies tailored toward antibiotic targets within complex matrices like environmental samples or biological fluids. Additionally, expanding upon this work may involve adapting these approaches towards multiplex detection systems that can simultaneously identify multiple contaminants or residues in food safety testing. By establishing clear correlations between fluorescence intensity from quantum dots and antibiotic concentrations while advancing methodologies in nanomaterial synthesis or surface engineering techniques, this novel approach offers promising alternatives to existing detection strategies while paving the way toward more sustainable practices concerning antibiotic monitoring in various settings.

Data availability

All data generated or analyzed during this study are included in this published article.

Received: 22 November 2024; Accepted: 11 February 2025
Published online: 28 March 2025

References

1. Bajorowicz, B. et al. Quantum dot-decorated semiconductor micro- and nanoparticles: A review of their synthesis, characterization and application in photocatalysis. *Adv. Colloid Interface Sci.* **256**, 352–372 (2018).
2. Singh, I., Arora, R., Dhiman, H. & Pahwa, R. Carbon quantum dots: Synthesis, characterization and biomedical applications. *Turk. J. Pharm. Sci.* **15**(2), 219–230 (2018).
3. Wang, R., Lu, K. Q., Tang, Z. R. & Xu, Y. J. Recent progress in carbon quantum dots: Synthesis, properties and applications in photocatalysis. *J. Mater. Chem. A* **7**(5), 3717–3734 (2017).
4. Nazri, N. A. A., Azeman, N. H., Luo, Y. & Bakar, A. Carbon quantum dots for optical sensor applications: A review. *Opt. Laser Technol.* **139**, 106928 (2021).
5. Pan, M. et al. Fluorescent carbon quantum dots-synthesis, functionalization and sensing application in foodanalysis. *Nanomaterials (Basel).* **10**(5), 930 (2020).
6. Sabzehmeidani, M. M. & Kazemzad, M. Quantum dots based sensitive nanosensors for detection of antibiotics in natural products: A review. *Sci. Total Environ.* **1**(810), 151997 (2022).
7. Zhou, T., Halder, A. & Sun, Y. Fluorescent nanosensor based on molecularly imprinted polymers coated on graphene quantum dots for fast detection of antibiotics. *Biosensors (Basel).* **8**(3), 82 (2018).
8. Ding, R. et al. Recent advances in quantum dots-based biosensors for antibiotics detection. *J. Pharm. Anal.* **12**(3), 355–364 (2022).
9. Pawar, S. P. et al. Fluorescence-based sensor for selective and sensitive detection of amoxicillin (Amox) in aqueous medium: Application to pharmaceutical and biomedical analysis. *Luminescence.* **32**(6), 918–923 (2017).
10. Sharma, A. et al. Nanomaterials in fluorescence-based biosensors: Defining key roles. *Nano-Struct. Nano-Objects.* **27**, 100774 (2021).
11. Brogden, R. N. & Campoli-Richards, D. M. Cefixime. A review of its antibacterial activity. Pharmacokinetic properties and therapeutic potential. *Drugs.* **38**(4), 524–550 (1989).
12. Kasrati, A. et al. Antioxidative activity and synergistic effect of Thymus saturejoides Coss. essential oils with cefixime against selected food-borne bacteriaInd. *Crops Prod.* **61**, 338 (2014).
13. Azmi, S. N. H., Iqbal, B., Al Mamari, J. K., Al Hattali, K. A. & Al Hadhrami, W. N. Method development and validation for the determination of cefixime in pure and commercial dosage forms by specrophotometry. *Int. J. Chem. Mol. Eng.* **8**, 595 (2014).
14. Graber, E. M. Treating acne with the tetracycline class of antibiotics: A review. *Dermatol. Rev.* **2**, 321 (2021).
15. Ahmed, S. R. et al. Electrochemical assisted enhanced nanozymatic activity of functionalized borophene for H2O2 and tetracycline detection. *Biosens. Bioelectron.* **246**, 115857 (2024).
16. Qureshi, T., Memon, N., Memon, S.Q., Abro, K., Shah, S.W. LC/UV determination of cefradine, cefuroxime, and cefotaxime in dairy milk, human serum and wastewater samples. *Springerplus.* **2**(575) (2013).
17. Kumar, U. et al. In-situ H2O2 production for tetracycline degradation on Ag/s-(Co3O4/NiFe2O4) visible light magnetically recyclable photocatalyst. *Appl. Surf. Sci.* **589**, 153013 (2022).
18. Sagar, P., Srivastava, M., Prakash, R., Srivastava, S.K. *Anal. Methods.* **12**(23), 3014–3024 (2020).
19. Abedi-Firoozjah, R. et al. State-of-the-art nanosensors and kits for the detection of antibiotic residues in milk and dairy products. *Adv. Colloid Interface Sci.* **328**, 103164 (2024).
20. Pérez-Rodríguez, M., Pellerano, R. G., Pezza, L. & Pezza, H. R. An overview of the main foodstuff sample preparation technologies for tetracycline residue determination. *Talanta.* **15**(182), 1–21 (2018).
21. Zheng, Y. et al. A water-stable terbium-based MOF fluorescence sensor for rapid and highly sensitive quantitative detection of cefixime. *Dye. Pigment.* **230**, 112340 (2024).
22. Das, P., Ganguly, S., Banerjee, S. & Das, N. C. Graphene based emergent nanolights: a short review on the synthesis, properties and application. *Res. Chem. Intermed.* **45**, 3823–3853 (2019).
23. Pongprom, A. & Bunkoed, O. A fluorescent nanocomposite probe of quantum dots and zinc oxide embedded in polymer for smartphone-assisted on-site determination of diflunisal. *Spectrochim. Acta A Mol. Biomol. Spectrosc.* **5**(326), 125243 (2025).
24. Chullasat, K., Kanatharana, P. & Bunkoed, O. Nanocomposite optosensor of dual quantum dot fluorescence probes for simultaneous detection of cephalexin and ceftriaxone. *Sensors Actuators B Chem.* **15**(281), 689–697 (2019).
25. De Ruyck, H. & De Ridder, H. Determination of tetracycline antibiotics in cow's milk by liquid chromatography/tandem mass spectrometry. *Rapid Commun. Mass Spectrom.* **21**(9), 1511–1520 (2007).

26. Salama, N. A., Abou-Raya, S. H., Shalaby, A. R., Emam, W. H. & Mehaya, F. M. Incidence of tetracycline residues in chicken meat and liver retailed to consumers. *Food Addit. Contam. Part B Surveill.* **4**(2), 88–93 (2011).
27. Pandiyarajan, T. & Karthikeyan, B. Cr doping induced structural, phonon and excitonic properties of ZnO nanoparticles. *J. Nanoparticle Res.* **14**, 647 (2012).
28. Lu, X. et al. Preparation and characterization of polyaniline microwires containing CdS nanoparticles. *Chem. Commun. (Camb.).* **13**, 1522–1523 (2004).
29. Madhavi, J., Prasad, V., Reddy, K. R., Reddy, C. V. & Raghu, A. V. Facile synthesis of Ni-doped ZnS-CdS composite and their magnetic and photoluminescence properties. *Chem. Eng.* **9**, 106335 (2021).
30. Manzar, M. S. et al. RSM-CCD optimization approach for the adsorptive removal of Eriochrome Black T from aqueous system using steel slag-based adsorbent: Characterization, Isotherm, Kinetic modeling and thermodynamic analysis. *J. Mol. Liq.* **339**, 116714 (2021).
31. Liang, N. et al. A dual-signal fluorescent sensor based on MoS2 and CdTe quantum dots for tetracycline detection in milk. *Food Chem.* **1**(378), 132076 (2022).
32. Hu, F. et al. Zinc-doped carbon quantum dots-based ratiometric fluorescence probe for rapid, specific, and visual determination of tetracycline hydrochloride. *Food Chem.* **15**(431), 137097 (2024).
33. Fan, Y. et al. Detection of tetracycline antibiotics using fluorescent "Turn-off" sensor based on S, N-doped carbon quantum dots. *Spectrochim. Acta A Mol. Biomol. Spectrosc.* **5**(274), 121033 (2022).
34. Haddad Irani-Nezhad, M., Jalili, R., Kohan, E., Khataee, A. & Yoon, Y. Tungsten disulfide (WS2)/fluorescein ratiometric fluorescent probe for detection of cefixime residues in milk. *Environ. Res.* **1**(205), 112512 (2022).
35. Eskandari, H., Amirzehni, M., Asadollahzadeh, H. & Eslami, P. A. Molecularly imprinted polymers on CdS quantum dots for sensitive determination of cefixime after its preconcentration by magnetic graphene oxide. *New J. Chem.* **41**(15), 7186–7194 (2017).
36. Wei, X. et al. Molecularly imprinted CsPbBr 3 quantum dot-based fluorescent sensor for trace tetracycline detection in aqueous environments. *J. Mater. Chem. C* **10**(21), 8432–8440 (2022).
37. Khawla, M., Zouhour, H., Yves, C., Souhaira, H. & Rym, M. ZnS quantum dots as fluorescence sensor for quantitative detection of tetracycline. *Opt. Mater. Amst.* **125**, 112103 (2022).
38. Wang, C. et al. Preparation of highly luminescent nitrogen-doped carbon quantum dots and their detection of tetracycline antibiotics. *Colloids Surfaces A Physicochem. Eng. Asp.* **653**, 129982 (2022).

Acknowledgements

We are grateful to the Department of Biology, Sanandaj Branch, Islamic Azad University, Sanandaj, Iran for their support for this work.

Author contributions

F.K. , CH.K. and SH.J. wrote the manuscript text, prepared figures. All authors reviewed the manuscript."

Funding

This research received no external funding.

Declarations

Competing interests

The authors declare no competing interests.

Additional information

Correspondence and requests for materials should be addressed to F.K.

Reprints and permissions information is available at www.nature.com/reprints.

Publisher's note Springer Nature remains neutral with regard to jurisdictional claims in published maps and institutional affiliations.